The Effect of Adding Roughness and Thickness to a Transonic Axial Compressor Rotor

K. L. Suder

R. V. Chima

A. J. Strazisar

NASA-Lewis Research Center,
Cleveland, OH 44135

W. B. Roberts

Flow Application Research and Sermatech International Inc.,
Fremont, CA 94539

The performance deterioration of a high-speed axial compressor rotor due to surface roughness and airfoil thickness variations is reported. A 0.025 mm (0.001 in.) thick rough coating with a surface finish of 2.54–3.18 rms μm (100–125 rms μin.) is applied to the pressure and suction surface of the rotor blades. Coating both surfaces increases the leading edge thickness by 10 percent at the hub and 20 percent at the tip. Application of this coating results in a loss in efficiency of 6 points and a 9 percent reduction in the pressure ratio across the rotor at an operating condition near the design point. To separate the effects of thickness and roughness, a smooth coating of equal thickness is also applied to the blade. The smooth coating surface finish is 0.254–0.508 rms μm (10–20 rms μin.), compared to the bare metal blade surface finish of 0.508 rms μm (20 rms μin.). The smooth coating results in approximately half of the performance deterioration found from the rough coating. Both coatings are then applied to different portions of the blade surface to determine which portions of the airfoil are most sensitive to thickness/roughness variations. Aerodynamic performance measurements are presented for a number of coating configurations at 60, 80, and 100 percent of design speed. The results indicate that thickness/roughness over the first 2 percent of blade chord accounts for virtually all of the observed performance degradation for the smooth coating, compared to about 70 percent of the observed performance degradation for the rough coating. The performance deterioration is investigated in more detail at design speed using laser anemometer measurements as well as predictions generated by a quasi-three-dimensional Navier–Stokes flow solver, which includes a surface roughness model. Measurements and analysis are performed on the baseline blade and the full-coverage smooth and rough coatings. The results indicate that adding roughness at the blade leading edge causes a thickening of the blade boundary layers. The interaction between the rotor passage shock and the thickened suction surface boundary layer then results in an increase in blockage, which reduces the diffusion level in the rear half of the blade passage, thus reducing the aerodynamic performance of the rotor.

Introduction

Industries that use gas turbine engines have a continuing need for data on in-service performance loss due to component deterioration. This need is especially great in the airline industry, for which fuel burn and performance retention in high bypass ratio turbofan engines is a major concern. The single component of a high-bypass engine that absorbs the greatest amount of energy and accounts for the greatest fuel burn is the transonic fan. Furthermore, fan blades suffer the most rapid erosion and surface roughening due to lower-atmosphere particulates and runway debris. If the performance effects of fan blade in-service deterioration can be quantified, cost-effective repair strategies and replacement intervals can be deduced (see the technical note by Roberts in this issue). In addition, understanding of the mechanisms by which blade deterioration degrades performance may allow manufacturers to develop design and manufacturing strategies aimed at minimizing long-term performance deterioration.

Engine component deterioration and overall loss in performance have been documented by a number of investigators, including Sallee et al. (1978), Kramer et al. (1980), Covey et al. (1978), and the DOE/FAA Symposium (1981). Since turbomachinery blading performance loss is generally attributed to increased surface roughness as well as particulate impact damage to blade leading edges, a number of investigators have studied the effect of surface roughness on blading performance. The effects of roughness on turbine aerodynamic performance have been investigated experimentally by Roelke and Haas (1983) and Boynton et al. (1993). Boyle (1994) recently predicted the efficiency loss due to roughness measured by Boynton by using a quasi-three-dimensional Navier–Stokes analysis in which he augmented a mixing length model to account for the effects of surface roughness. The effect of roughness on compressor blade aerodynamic performance was reported by Moses and Serovy (1951), who documented the performance changes that resulted from polishing an initially rough blade. Reid and Urasek (1973) investigated the effect of leading edge thickness by documenting the change in performance of a transonic axial-flow fan as a result of cutting back the rotor leading edge. While documenting that roughness and leading edge thickness have an impact on the aerodynamic performance of turbomachinery blading, these previous investigations have not provided a definitive explanation of the mechanism through which roughness impacts performance.

The present investigation was triggered by the application of a special antireflective paint to a transonic compressor rotor. The paint derived its antireflective properties from the presence of small silica particles embedded in the paint, which create a rough surface that diffuses rather than reflects incident light. The paint was applied during the laser anemometer investigation

Contributed by the International Gas Turbine Institute and presented at the 39th International Gas Turbine and Aeroengine Congress and Exposition, The Hague, The Netherlands, June 13–16, 1994. Manuscript received by the International Gas Turbine Institute March 2, 1994. Paper No. 94-GT-339. Associate Technical Editor: E. M. Greitzer.

of the rotor flow field reported by Suder and Celestina (1994) in an attempt to suppress laser light reflections from the blading. However, the painted rotor suffered a significant deterioration in performance, with pressure ratio dropping by 9 percent and efficiency dropping by 6 points at an operating condition near the design point. When the paint was removed, the aerodynamic performance returned to its previous level. As a result, the anemometer optics and electronics were modified to reject light reflected from the blading, and the paint was not used by Suder and Celestina while acquiring laser anemometer measurements.

Comparison of surface finish measurements from the painted test rotor and a typical aircraft gas turbine engine fan blade prior to blade refurbishment showed that the antireflective paint provided roughness levels that were a reasonable model of in-service roughness levels. Therefore, at the conclusion of the previous test program, the paint was once again applied to the rotor to study the effects of roughness on performance deterioration.

Figure 1 shows a comparison of the fan blade leading edge and the test rotor leading edge with the rough paint applied. There are two important differences between the in-service damage observed on the engine fan blade and the roughness applied to the research rotor in this experiment. First, the fan blade leading edge is visibly pitted due to particle impact, as can be seen in Fig. 1(*b*), while the research rotor leading edge is not pitted. The coatings applied to the research rotor were much softer than the blade itself and did suffer impact damage at the leading edge during testing. However, we did not measure nor did we attempt to control the level of this impact damage. Second, in-service damage generates surface roughness by removing material from the blade, but in this investigation we are creating surface roughness by adding material to the blade. In drawing conclusions on in-service performance deterioration based on the results presented herein, one must therefore assume that performance deterioration is dependent on the roughness level but is independent of how the roughness was created.

Both smooth and rough paint coatings were applied to the entire blade surface in an attempt to separate the effects due to adding thickness to the blade from those due to adding surface roughness to the blade. Both coatings were then applied to different portions of the blade surface to determine which portions of the airfoil were most sensitive to thickness/roughness variations. Aerodynamic performance measurements are presented for a number of smooth and rough coating configurations at 60, 80, and 100 percent of design speed to quantify the performance sensitivity to thickness and roughness variations over a wide range of operating conditions.

The largest degradation in performance occurred at the design speed operating condition when the entire blade surface was coated. As a result, the baseline (bare metal) rotor, full-coverage smooth coating, and full-coverage rough coating cases were selected for further investigation. Detailed laser fringe anemometer (LFA) measurements were acquired at design speed for these three cases. LFA measurements were acquired upstream, within, and downstream of the blade.

Flow field predictions generated with a quasi-three-dimensional Navier–Stokes flow solver were used to complement the LFA measurements by providing insight into the flow development in regions near the blade leading edge and near the blade surface where LFA data could not be acquired. The viscous analysis code featured a **C**-grid for accurate resolution of the

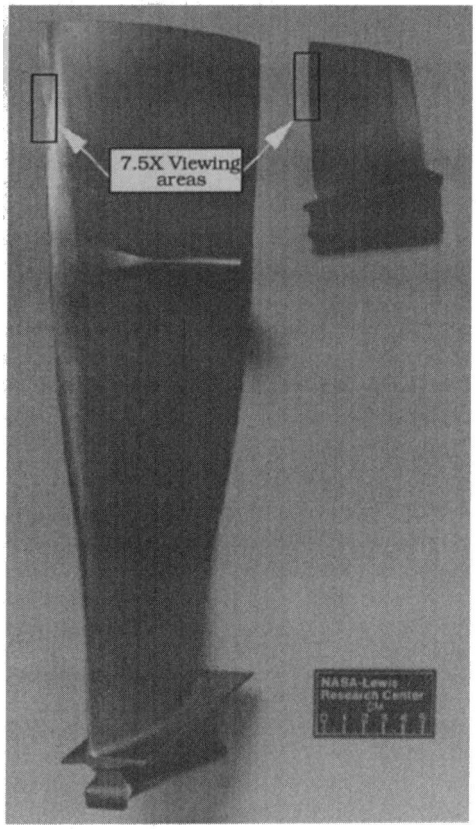

Fig. 1(*a*) Comparison between engine fan blade and the research rotor blade

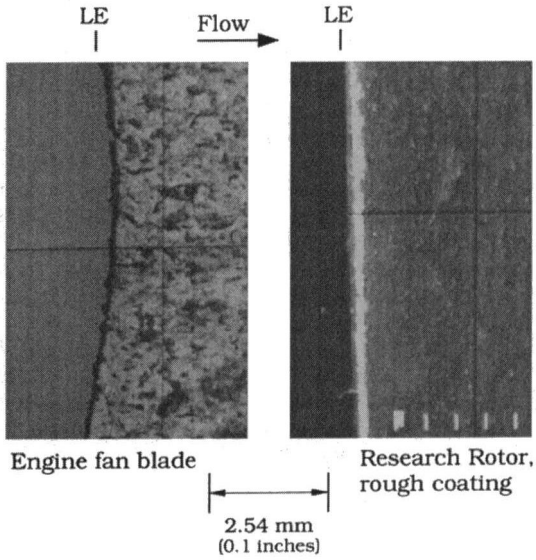

Fig. 1(*b*) 7.5× view of fan blade and coated research rotor leading edges

Nomenclature

H = total enthalpy
$\dot{m}$ = massflow rate, kg/s
M_{rel} = relative Mach number
P_4 = total pressure at Station 4; see Fig. 2
PR = total pressure ratio
P_{ref} = standard-day total pressure = 101,325 n/m^2
ps = denotes pressure surface
r = radius, m
ss = denotes suction surface
T_4 = total temperature at Station 4; see Fig. 2
T_{ref} = standard day total temperature, 288.2 K

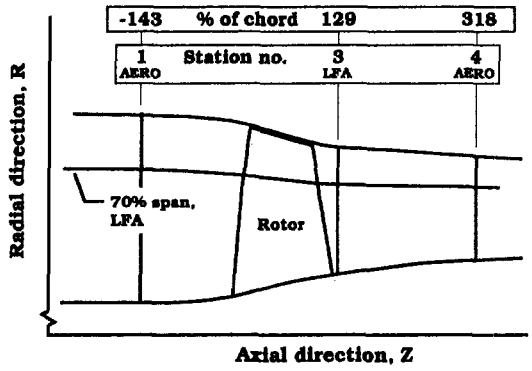

Fig. 2 Laser anemometer and aerodynamic survey stations

leading edge region and included a surface roughness model. Analysis was performed on the baseline blade, on a blade profile with added thickness with and without added roughness, and on a blade profile with a noncircular leading edge.

Test Compressor

The test compressor for the present study is a low-aspect-ratio transonic core compressor inlet stage, designated NASA Stage 37. The results reported here were obtained from a rotor-only configuration with the stator removed. This configuration eliminates blade row interactions and thus allows comparison of the measurements with numerical predictions based on circumferentially uniform upstream and downstream conditions.

The rotor design pressure ratio is 2.106 at a mass flow of 20.19 kg/s. The inlet relative Mach number is 1.13 at the hub and 1.48 at the tip at the design tip speed of 454 m/s. The rotor aspect ratio is 1.19 and the hub/tip radius ratio is 0.70. The rotor tip clearance at design speed is 0.40 mm (0.016 in.), which corresponds to 0.7 percent of chord. Details of the rotor aerodynamic design were reported by Reid and Moore (1978). Overall aerodynamic performance of the stage was reported by Moore and Reid (1980).

Instrumentation and Measurement Techniques

Massflow is measured using a calibrated orifice located far upstream of the compressor. The orifice measurements are corrected to standard-day conditions at the rotor inlet. Radial distributions of total and static pressure, total temperature, and flow angle are measured at stations 1 and 4 shown in Fig. 2. Stage 37 is a close-coupled stage, and there is not sufficient space for a survey station between the rotor and stator. Since additional survey stations were not added in the present work, Station 4, which is normally used to survey the stator outlet flow, is the first available aerodynamic survey station downstream of the rotor. The measurement uncertainties are: massflow, ±0.3 kg/s; flow angle, ±0.5 deg; total pressure, ±0.01 N/cm^2; total temperature, ±0.6 K. The probe measurements are corrected for Mach number and streamline slope based on a calibration of each probe used and on the design streamline slope. All measurements are corrected to sea-level standard-day conditions at the rotor inlet. Radial distributions of total temperature are mass averaged across the annulus. Radial distributions of total pressure are energy averaged by converting them to their enthalpy equivalents and then mass averaging them across the annulus.

A laser fringe anemometer system (LFA) is used to obtain detailed flow field velocity measurements. This instrument is a two-channel system configured to provide simultaneous measurements of the axial and tangential velocity components. Optical access to the compressor is provided by a 2.5-mm-thick glass window, which conforms to the shroud contour, thus preserving the proper tip clearance over the rotor. Polystyrene latex seed particles are injected into the flow field far upstream of the test compressor to enable LFA measurements. These particles are manufactured using the process developed by Nichols (1987) and their size is determined using scanning electron microscope (SEM) photographs. The range of particle sizes used in the present investigation is 0.7–0.9 μm. The SEM photographs indicate that although the particle size varies within this range between batches, the size within a given batch is uniform to within 0.1 μm. Particle batches were not mixed during research runs. Therefore, all LFA data were acquired with uniformly sized particles, although the mean particle size varied between 0.7–0.9 μm. The error in the LFA measurements is approximately 1 m/s for absolute velocity and 0.5 deg for absolute flow angle and is independent of the particle size over the size range used. Further details concerning the LFA system and measurement technique are reported by Suder and Celestina (1994).

LFA data were acquired from hub to tip downstream of the rotor at Station 3, shown in Fig. 2, to provide an assessment of roughness/thickness effects at a location close to the rotor trailing edge. LFA data was also acquired on the blade-to-blade streamsurface at 70 percent span shown in Fig. 2. The choice of the 70 percent span location was driven by several factors. First, aerodynamic performance measurements acquired for the coated blade indicated that at design speed the degradation in pressure and temperature rise was largest near the tip of the blade. Second, previous LFA data acquired in this rotor indicated the tip clearance flow penetrates to at least 90 percent span, causing a steep gradient in flow properties across the outer 10 percent of blade span. Finally, LFA data had already been acquired for the baseline blade at 70 percent span during previous testing of this rotor. The 70 percent span streamsurface was therefore chosen as a compromise between our desire to survey the flow field near the tip of the blade and our desire to survey the flow field at a spanwise location at which radial gradients in flow properties were not too strong.

Measurements within the blade passage were acquired at axial intervals of 5 percent chord. At each axial/radial measurement location, data were acquired across all 36 blade passages at a circumferential resolution of 184 points across one blade pitch. All LFA results presented in this paper represent the flow field within an averaged blade passage, which was calculated by ensemble-averaging the measurements acquired in each individual blade passage.

The relative Mach number is calculated from the relative velocity and the local speed of sound at each point in the flow field using the procedure discussed by Strazisar et al. (1989). All Mach numbers presented in this report are "two-dimensional" Mach numbers in that they are calculated ignoring the radial velocity component, which cannot be measured by the LFA system. Suder and Celestina (1994) have calculated the Mach numbers in rotor 37 with and without the radial velocity component using a three-dimensional Navier–Stokes flow field solution and found that ignoring the radial velocity component led to a maximum error of 2 percent in relative Mach number.

Experimental Procedure

Coating Application and Inspection. All coatings used in this investigation were applied to the blade surface with a brush using spanwise brush strokes, which provided a uniform coating thickness around the blade leading edge. Chordwise brush strokes were not used since they tended to scrape paint from the brush onto the leading edge, resulting in poor control of the coating thickness at the leading edge. When only part of the blade was coated, a template was used to insure that all blades were painted over a given chordwise area from hub to tip. A flat aluminum plate was coated with the same paint using the same brush that was used on the blades and the paint film

Table 1 Comparison of coating thickness as measured by various techniques

Meas. Method	Accuracy mm (in.)	Gauge block paint thickness, mm (inches)		
		Minimum	Maximum	Average
Micrometer	0.005 (0.0002)	0.028 (0.0011)	0.064 (0.0025)	0.046 (0.0018)
Comparator	0.012 (0.0005)	0.041 (0.0016)	0.043 (0.0017)	0.042 (0.0016)
Eyelash machine	0.025 (0.001)	0.025 (0.001)	0.051 (0.002)	0.038 (0.0015)

Table 2 The rms surface finished for engine fan blade and rotor 37 blade

Configuration	RMS surface finish		Equivalent sand roughness Reynolds No.
	microns	μin.	
Rotor 37, baseline blade	0.508	20	93
Rotor 37, smooth coating	0.254–0.508	10-20	47-93
Rotor 37, rough coating	2.54–3.18	100-125	470-580
fan blade, pressure surface	4.31-6.10	170-240	960-1350
fan blade, suction surface	1.14-1.65	45-65	250-370

thickness was measured using a micrometer. The paint thickness on the test plate varied from 0.017 mm (0.0007 in.) to 0.030 mm (0.0012 in.) for both rough and smooth coatings.

At the conclusion of the test program, several blades painted with the rough coating were inspected in an eyelash machine to determine the uniformity of the coating on the actual blades. After inspecting a painted blade, the paint was removed while the blade was mounted in the eyelash machine and the blade was re-inspected, thus providing back-to-back inspections to determine the in-situ coating thickness. The eyelash inspections indicated that the paint film on the blade surface ranged in thickness from 0.013–0.025 mm (0.0005–0.0010 in.). The ability of the eyelash machine to measure the painted blade accurately was assessed by painting a gage block and determining the paint thickness using a micrometer, an optical comparator, and the eyelash machine. The accuracy of each measurement technique and the coating thickness measured with each technique are shown in Table 1.

Note that the average micrometer reading was high compared to that of the comparator and that the eyelash machine was performing at the limits of its resolution. Based on this calibration exercise, the test plate inspections, and the blade eyelash inspections, we conclude that the coating thickness on each surface of the blade was nominally 0.025 mm (0.001 in.) and was certainly no greater than 0.050 mm (0.002 in). A coating thickness of 0.025 mm on the blade pressure and suction surface corresponds to 10 percent of the leading edge thickness at the hub, to 20 percent of the leading edge thickness at the tip, and to only 0.3 percent of the throat width at the blade tip. Furthermore, the amount of thickness added to the blade surfaces by the coatings was well within the overall blade thickness manufacturing tolerance of ±0.125 mm (0.005 in.), and is comparable to the leading edge blade thickness manufacturing tolerance of ±0.050 mm (0.002 in.).

The results of the eyelash inspection for a single blade at 90 percent span coated with rough paint are shown in Fig. 3. A circle of arbitrary diameter has been fit to the blade leading edge simply to help gage the degree to which the leading edge is not circular. For this blade at this radius the coating actually tends to make the leading edge more circular than it is for the bare metal blade. The figure also shows that a relatively sharp shoulder exists for both the smooth and coated blade where the leading edge blends into the suction surface. The impact of such a shoulder on the flow development along the blade was investigated computationally, and the results will be discussed later.

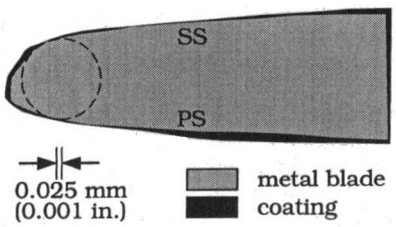

Fig. 3 Eyelash inspection results for a rough-coated blade at 90 percent span; ss = suction surface; ps = pressure surface

The nominal rms surface finishes determined with a profilometer are shown in Table 2. Also listed in the table are surface finish readings from the engine fan blade shown in Fig. 1 and the equivalent roughness Reynolds numbers, calculated following the method of Koch and Smith (1975). According to Koch and Smith, the blade surface is considered hydraulically smooth for roughness Reynolds numbers less than 90.

Aerodynamic Performance Measurements. Aerodynamic performance measurements were acquired for the baseline and fully coated configurations at 60, 80, and 100 percent of design speed. The relative inlet Mach numbers for each speed are given in Table 3. These three speeds were chosen to investigate the correlation between Mach number and performance deterioration due to roughness/thickness. At design speed the relative flow is supersonic from hub to tip. At 80 percent of design speed the relative flow is transonic, which is typical of low hub/tip ratio fans. At 60 percent of design speed, the relative flow is subsonic everywhere, which is more characteristic of middle- and exit-stage core compressor blading.

The coating configurations and the measurements acquired for each configuration are summarized in Table 4. The column labeled "coating configuration" summarizes the area of the suction and pressure surface (denoted as ss and ps respectively), which was coated. For example, case D featured a coating that was applied from 2–10 percent chord on both the pressure and suction surface. Case A corresponds to a single coat of smooth paint, with a nominal thickness of 0.0125 mm (0.0005 in.). The nominal coating thickness for all other cases is 0.025 mm (0.001 in.).

Aerodynamic performance measurements were first acquired for the bare metal rotor at 60, 80, and 100 percent of design speed to establish baseline aerodynamic performance. The blades were then coated over their entire surface with the rough paint (case I) and the aerodynamic measurements were repeated to document performance degradation. The coating was then removed using a solvent and wire brush, and the aerodynamic performance measurements on the bare metal blade were re-

Table 3 Rotor 37 inlet relative Mach numbers

% speed	M_{rel} at hub	M_{rel} at tip
60	0.68	0.89
80	0.90	1.18
100	1.13	1.48

Table 4 Summary of coating configurations and aerodynamic survey conditions

I.D.	Coating configuration		Coating type	Speed surveyed (% design)
	ps (%chord)	ss (%chord)		
A	0-100	0-100	smooth (1/2 thick)	60,80,100
B	0-100	0-100	smooth	60,80,100
C	0-10	0-10	smooth	100
D	2-10	2-10	rough	100
E	- - -	20-30	rough	100
F	2-100	55-100	rough	100
G	0-10	0-10	rough	100
H	0-10	0-50	rough	100
I	0-100	0-100	rough	60,80,100

peated. These measurements agreed with the baseline performance measurements to within measurement accuracy, thus verifying that the process of applying and removing the rough coating had not altered the rotor performance.

By applying a rough coating to the blade we added both thickness and surface roughness to the baseline blade. To separate the effects due to thickness from those due to surface roughness, a smooth coating of polyurethane was applied over the entire blade, thereby adding thickness without adding roughness. It was found that two coats of polyurethane were required to develop a coating thickness equal to that of the rough paint. Aerodynamic performance measurements were obtained at 60, 80, and 100 percent of design speed for both a single coating of polyurethane (case A) and a double coating (case B). At the completion of these measurements the blade was once again cleaned and the baseline aerodynamic performance was once again verified.

To determine which regions of the blade surface contributed most to the observed performance degradation, additional measurements were acquired for a number of partially coated configurations (cases C through H). All partially coated configurations were investigated only at design speed, since the performance degradation at design speed for the fully coated blade was much larger than the degradation observed at part-speed conditions. After measurements were completed on each configuration, the blade was cleaned and the baseline aerodynamic performance was spot-checked for repeatability at several points along the design speed operating line.

Aerodynamic Performance Results

Fully Coated Configurations. The smooth- and rough-coated performance is compared to the baseline performance in Figs. 4 and 5. The data points surrounded by circles in Fig. 4 indicate those points for which detailed radial distributions of flow properties will be discussed later. The results in Fig. 4 raise a question as to whether the degradation scales with tip speed. To address this issue, we normalized the pressure rise with tip speed and plotted this quantity against massflow. The results, which are not shown here, also indicated a significantly larger degradation at design speed than at part-speed conditions. Therefore, neither pressure ratio nor pressure rise scale with tip speed. This indicates that the rotor shock system, which generates much of the pressure rise at design speed, plays an important role in the degradation in pressure rise capability at design speed.

The stall line is not affected by coating the blades, but the maximum massflow achieved by the coated rotor is lower than that of the baseline rotor at all speeds. However, at design speed the highest massflows presented in Fig. 4 correspond to choking

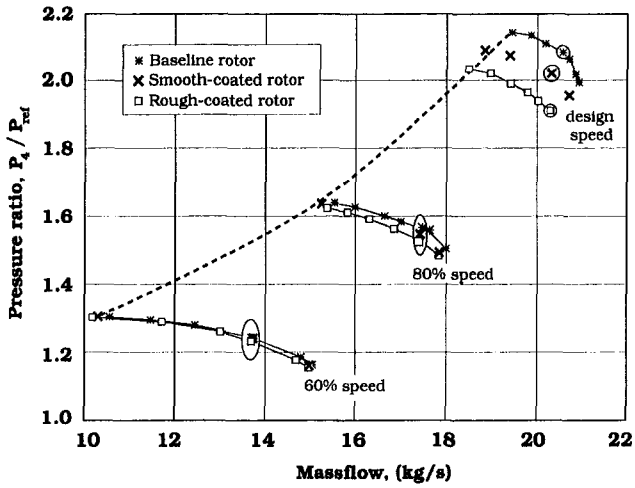

Fig. 4 Pressure rise characteristics for full-coverage coatings; circled points indicate operating conditions for which radial distributions of flow properties are presented

of the facility diffuser located between the rotor and the throttle valve, rather than choking of the rotor itself. Diffuser choke occurred prior to rotor choke because the diffuser was designed to accept the axial outflow of stage 37 rather than the swirling outflow of rotor 37. Subsequent testing with the stator in place, which removes the rotor outlet flow swirl before the flow enters the diffuser, has verified that the isolated rotor configuration was choked at 60 and 80 percent speed but was not choked at design speed.

The results shown in Fig. 5 indicate that for a given massflow the efficiency penalty for the coated rotor configurations is on the order of 1–3 points at 60 percent speed, 0.5–2 points at 80 percent speed, and 2.5 points at design speed. Note that the efficiency penalty at design speed is not much larger than that at 60 percent speed. In addition, the efficiency levels measured for the smooth and rough coatings are nearly identical. This fact suggests that the efficiency is adversely impacted by the addition of thickness alone, and that the surface roughness level used in the present investigation does not have an appreciable impact on efficiency. However, this conclusion is misleading since both the pressure ratio and efficiency are changing.

A clearer view of the efficiency changes at design speed is shown by plotting efficiency against pressure ratio, as shown in Fig. 6. With both efficiency and pressure ratio changing appreciably, it seems appropriate to assess the efficiency penalty

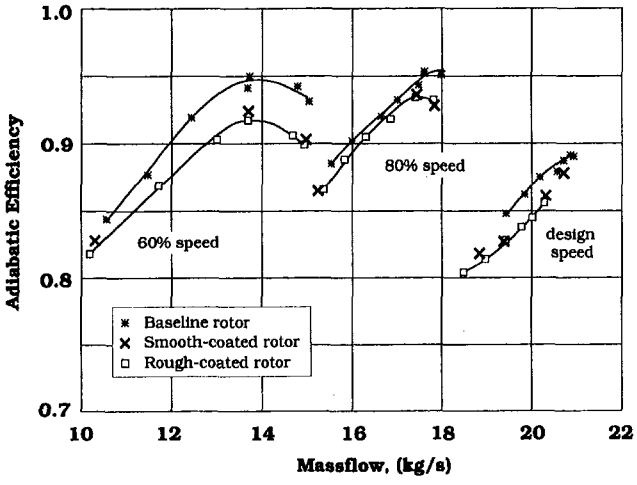

Fig. 5 Efficiency characteristics for full-coverage coatings

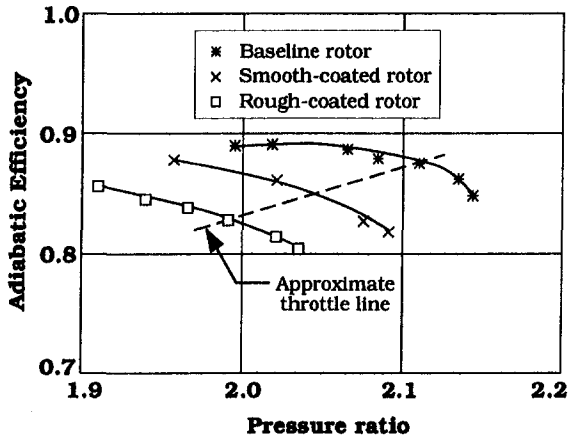

Fig. 6 Efficiency pressure ratio characteristics at design speed

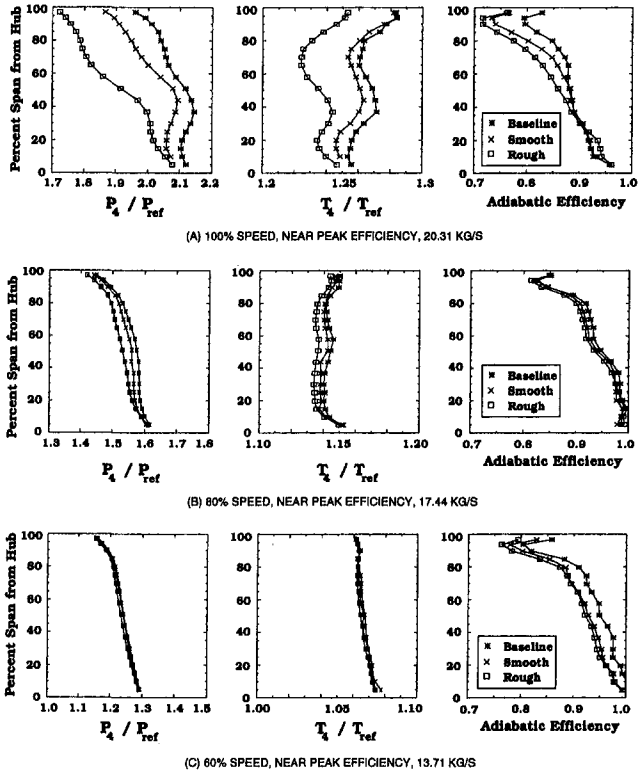

Fig. 7 Radial distributions of pressure ratio, temperature ratio, and efficiency

for both a constant pressure rise and a constant throttle resistance. For a constant pressure rise, the efficiency loss is on the order of 2.5–6.5 points for the smooth coating and 6–8.5 points for the rough coating. These loss levels would be experienced in compressor applications that require a constant pressure rise, such as pipeline pumping and stationary power generation. In contrast, aircraft engine fans and compressors operate against a fixed throttle resistance, and the operating point will move along a constant-throttle line as the compressor deteriorates in service. An approximate throttle line is shown in Fig. 6. The efficiency loss along this line is 2.5 points for the smooth coating and 5 points for the rough coating.

Figure 7 illustrates the spanwise variation of pressure ratio, temperature ratio, and adiabatic efficiency for the circled operating points shown in Fig. 4. The massflow chosen for comparison of the baseline and coated configurations at 60 and 80 percent speed corresponds to the peak efficiency massflow for the baseline rotor. At design speed, the massflow chosen corresponds to the maximum massflow achieved by the rough-coated rotor. Note that by comparing the baseline and coated blade performance at a constant massflow for each speed, we are maintaining a constant incidence angle for the performance comparison at a given speed.

The spanwise variation of flow properties measured at 100 percent of design speed is shown in Fig. 7(*a*). Note that for the smooth coating the degradation in pressure ratio is relatively constant below 50 percent span, but then nearly doubles in level between midspan and the tip. Also note that the efficiency penalty for the coated blades only becomes appreciable outboard of 40–60 percent span. Alber et al. (1973) have shown that for $M_{rel} \geq 1.4$, the pressure rise through a normal shock is strong enough to cause boundary layer separation. At design speed, the inlet relative Mach number for Rotor 37 varies from 1.13 at the hub to 1.48 at the tip. However, due to expansion along the suction surface, the Mach number at the face of the passage shock is greater than 1.4 outboard of midspan, and a strong shock/boundary layer interaction is therefore possible over the outer half of the blade span. These facts, coupled with the results shown in Fig. 7(*a*), indicate that the shock boundary layer interaction is an important contributor to the design speed performance degradation. This point is investigated in more detail later in this paper.

The spanwise variation of flow properties at 80 and 60 percent speed is shown in Figs. 7(*b*) and 7(*c*). The rotor shock system is quite weak at 80 percent speed and is only present in the outer half of the span. The performance decrement at part-speed conditions is much smaller than at design speed and more uniform in magnitude across the span. These results suggest that at lower Mach numbers, the coating effect on the blade surface boundary layers is the important flow phenomenon and that this effect is much weaker than the shock/boundary layer interaction effects that occur at design speed.

Partially Coated Configurations. Modern aircraft fans and compressors often operate under supersonic relative flow conditions over part of the blade span. The high Mach number results of the current study are therefore of particular interest. Since the preceding results have shown that the largest deterioration in rotor pressure rise occurs at design speed, we decided to coat various regions of the blade surface with smooth and rough coatings and acquire additional performance measurements at design speed to determine those areas of the blade surface that display the greatest sensitivity to the addition of thickness and roughness.

The results of the partial-coating study are shown in Figs. 8 and 9 for the nine coating configurations listed in Table 4. For

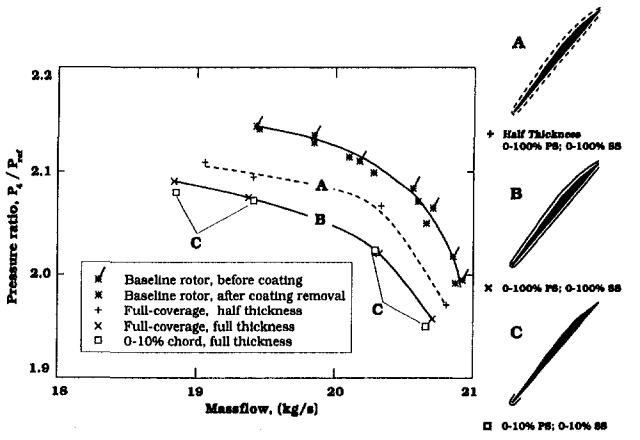

Fig. 8 Pressure rise characteristics for the smooth coatings at design speed

the baseline performance in both figures, the flagged data points were measured before any coatings were applied, while the unflagged points were measured on several different occasions after removal of coatings. The agreement between the flagged and unflagged points indicates that the baseline blade performance was not affected by the continued application and removal of coatings.

The pressure rise characteristics for the smooth-coated configurations A–C are compared to those of the baseline rotor in Fig. 8. Coatings A and B are full-coverage coatings with coating A being only half as thick as all other coatings. Coating C covers only the first 10 percent of blade chord. It can be seen that performance for the half thickness coating falls approximately halfway between that of the baseline and full thickness coating. However, the most dramatic result in Fig. 8 is that the performance deterioration for case C, in which only the leading edge region is coated, is virtually identical to that of case B in which the entire blade is coated. This result indicates that the added blade profile thickness from 10–90 percent chord does not contribute to the performance deterioration observed for Case B.

Figure 9 shows the decrease in design speed pressure ratio for rough coating configurations D–I listed in Table 4. The lowest massflows shown for cases G and H do not reflect the stall massflow—the stall point was simply not determined for these cases. As expected, the full coverage of rough paint, case I, gives the greatest deterioration in performance. This coating was applied on two separate occasions and yielded identical performance characteristics, thereby verifying the repeatability of the hand-application coating process. Case G, in which only the first 10 percent of chord is coated, exhibits approximately 70 percent of the performance degradation of the full roughness coverage. In case H the suction surface is coated up to the point at which the rotor passage shock impinges on the suction surface. Cases G, H, and I together indicate that the addition of roughness to the blade leading edge and the suction surface up to the point of shock impingement accounts for most of the performance degradation seen for the fully coated blade.

Cases D, E, and F all feature partial coatings, which did not cover the leading edge of the blade. Case D is similar to Case G except that the first 2 percent of the blade chord is not coated. Case E represents an attempt to trip the suction surface boundary layer by adding a strip of roughness in the high Mach number region between 20–30 percent chord. This case shows virtually no performance deterioration relative to the baseline blade.

Further discussion of the partial coating results will be easier if we can summarize the information in Figs. 8 and 9 in a single, quantitative format. Figure 10 summarizes the degradation in design speed pressure ratio as a function of the blade surface area covered by the full-thickness smooth and rough coatings. The plot abscissa represents an "unwrapped" blade surface with the blade leading edge at the center. The plot ordinate is the percent reduction in pressure ratio, defined as

$$100 * \frac{(PR)_{\text{baseline}} - PR}{(PR)_{\text{baseline}}}$$

The shaded bars represent the coated areas of the blade surface for each case. The results are shown for a massflow of 20.3 kg/s. This is the highest massflow reached for case I in Fig. 9. It is also the massflow used for the comparisons in Fig. 7, and is near the baseline rotor design point massflow of 20.19 kg/s.

After studying the results shown in Fig. 10 for cases B–I, it became clear to us that coating just the leading edge was an important case that we had not run. We therefore applied the smooth and rough coatings to the leading edge by running a brush along the leading edge. These coatings were applied after a stator had been installed behind the rotor. The stage with the coated rotor leading edge was run at a massflow of 20.3 kg/s, and the results are labeled "stage, le smooth" and "stage, le rough" in Fig. 10.

Figure 10 illustrates the magnitude of the performance degradation at a fixed flow rate while Figs. 8 and 9 illustrate that the level of degradation is not strongly dependent on the flow rate. The following conclusions for the design speed condition can be drawn from these results:

1 There is little performance degradation when the leading edge is left uncoated (Cases D, E, F).
2 Performance degradation is triggered by additional thickness and/or roughness at the leading edge.

- Cases D and G are geometrically similar except that Case D has no coating at the leading edge (0–2 percent chord). Case G exhibits performance degradation while Case D does not, which suggests that the coating on the first 2 percent of chord is the cause of the degradation observed for case G.
- Cases B and C exhibit identical degradation levels even though Case C is uncoated over much of the blade surface.
- The coated leading edge cases run in the stage configuration ("stage, le rough" and "stage, le smooth") display degradation levels that are similar to those of cases C and G (first 10 percent of chord coated) run on the isolated rotor
- Case G (first 10 percent of surface coated) exhibits 70 percent of the degradation level of Case I (entire surface coated).

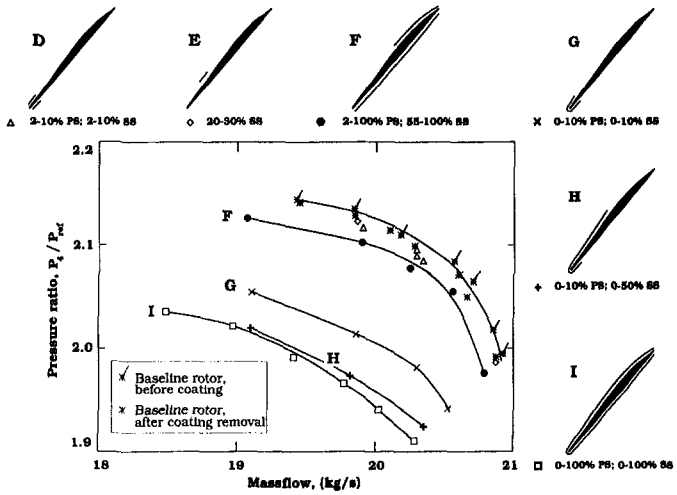

Fig. 9 Pressure rise characteristics for the rough coatings at design speed

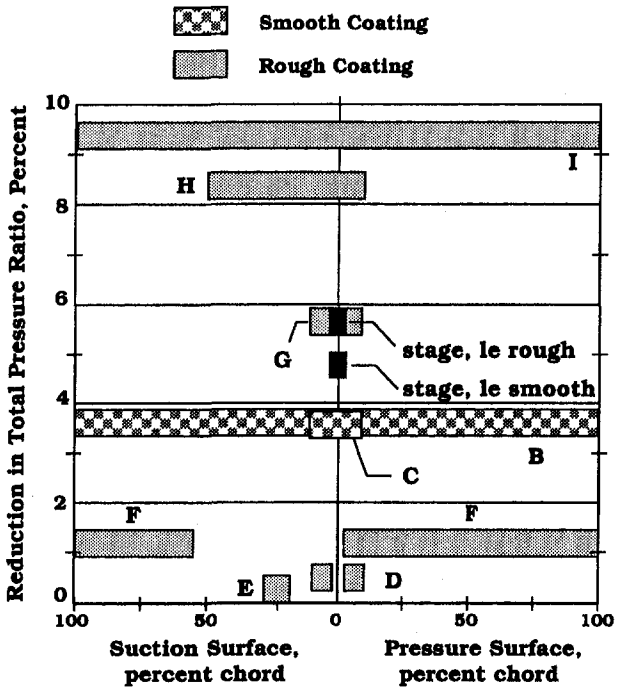

Fig. 10 Pressure ratio degradation as a function of blade surface area covered by smooth and rough coatings at design speed; massflow = 20.3 kg/s

3 Pressure surface roughness has little impact on performance degradation.

- Case F, in which the entire pressure surface was coated, demonstrates little degradation.
- There is little difference in degradation between cases H and I. The pressure surface is completely coated for case I and is uncoated from 10–100 percent chord in Case H.

4 Roughness on the uncovered portion of the suction surface has an impact on performance degradation.

- Cases G and H differ only in the extent of the roughness on the suction surface.

The results shown in Fig. 10 clearly indicate that the leading edge region plays a critical role in the performance degradation and that coating the leading edge results in performance loss. In coating the leading edge we increased its thickness by 10 percent at the hub and by 20 percent at the tip. Both the smooth and rough coatings had a lower surface hardness than the bare metal blade. As a result, coating the blade also increased the roughness at the leading edge because the coated blades suffered particle impact damage at the leading edge during testing that was not suffered by the baseline metal blade. We cannot separate the effects due to increased leading edge thickness from those due to increased leading edge roughness based on the measurements alone. However, the numerical analysis presented later in this paper indicates that the observed performance degradation is *not* a thickness effect.

Laser Anemometer Results

All LFA data reported herein were acquired at design speed for the baseline blade as well as the full-coverage smooth and rough coating configurations (cases B and I) at 70 percent span. The pressure ratio versus massflow characteristics for the 70 percent span streamsurface for these three cases are shown in Fig. 11. The massflow at which LFA data were acquired for each case is shown by the circled symbols. The characteristics are shown for the 70 percent span streamsurface to facilitate comparison to the CFD predictions made on the same streamsurface. The massflow and pressure ratio have been normalized by their respective maximum values for the baseline blade for the same reason.

Spanwise Velocity Distributions. The aerodynamic performance measurements presented above were based on measurements acquired with aerodynamic survey probes at Station 4 (see Fig. 2). Since Station 4 was two rotor chords downstream of the trailing edge, there was some concern that mixing that occurs between the rotor trailing edge and Station 4 might cause the aerodynamic measurements to provide an inaccurate view of the effects of roughness/thickness variations on rotor performance. LFA data were therefore acquired at Station 3, close to the rotor exit, for comparison with the aerodynamic survey measurements obtained far downstream at Station 4. The measured total temperature rise was chosen for this comparison since it is a measure of the work input across the rotor.

The Euler equation for turbomachinery was used to calculate the radial distribution of total temperature at Station 3 from the LFA velocity measurements. Figure 12 is a comparison between the aerodynamic probe measurements at Station 4 and the pitch-averaged total temperature ratios determined from the LFA measurements at Station 3. Comparison of the temperature distributions in Fig. 12 indicates that the temperature changes measured by the aerodynamic survey probes at Station 4 are qualitatively similar to those calculated from the LFA measurements near the trailing edge. In both cases the coatings cause a decrease in temperature rise across the entire blade span. The aerodynamic performance measured by the probes at Station 4 is therefore taken to be an accurate representation of the rotor performance.

Blade-to-Blade Flow Details. Figure 13 illustrates the distribution of local relative Mach number determined from the LFA measurements on the 70 percent span streamsurface for the baseline, smooth-coated, and rough-coated blades. The Mach number contour increment is 0.10. The shaded area in the lower blade passage in each contour plot indicates the area downstream of the shock for which the Mach number is greater than 0.90. The inset shows the shock location, as defined by the M_{rel} = 1.3 contour line, for each case. The 20, 40, 65, 90, and 115 percent chord locations are also noted because blade-to-blade distributions of Mach numbers at these locations will be presented below.

The Mach number distributions upstream of the shock are quite similar. The passage shock angle is slightly more oblique

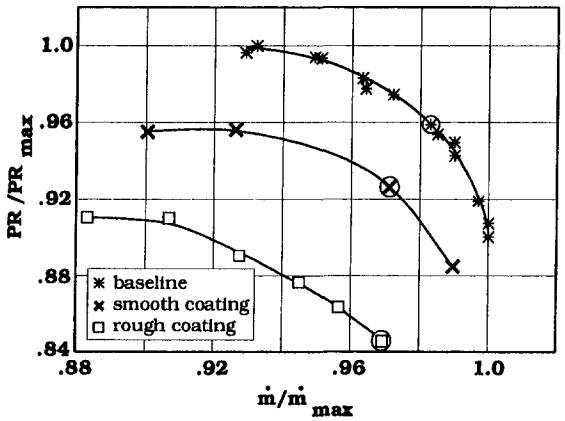

Fig. 11 Pressure ratio versus massflow characteristics at 70 percent span; circled points indicate operating conditions during laser anemometer surveys

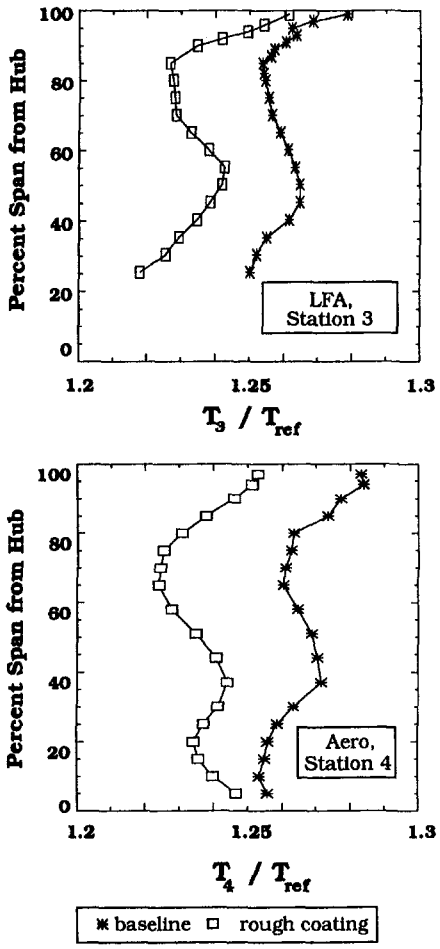

Fig. 12 Comparison between temperature ratios measured near the rotor trailing edge with the LFA and far downstream with aerodynamic survey probes

for the baseline case compared to the coated cases, but this is attributed more to the baseline data being acquired at a slightly higher massflow (see Fig. 11) than to flow field changes caused by coating the blade. The shock stand-off distance from the blade leading edge changes very little between the baseline and coated blade cases. This agrees with data presented by Liepmann and Roshko (1967) on the stand-off distance for circular cylinders as a function of cylinder diameter and Mach number. Although the coatings increased the leading edge thickness by 15 percent at 70 percent span, the cylinder data indicate that the expected change in stand-off distance for this thickness change at a Mach number of 1.4 is only one-half of the leading edge diameter.

The similarities in the flow fields ahead of the shock are consistent with the fact that the massflow, and therefore the incidence angle, is nearly the same for all three cases. Since the shock geometry is similar, the question remains as to why the pressure rise across the rotor varies considerably for these three cases. The pressure rise across the shock accounts for much of the overall pressure rise across the rotor, and the loss in pressure rise for the coated cases must therefore be due to changes in the flow field downstream of the shock. Both coated cases display a more prominent lambda shock foot than the baseline case, followed by a region of low Mach number along the suction surface downstream of the shock impingement point. This behavior is not observed in the baseline blade Mach number distribution. These results indicate that the shock/boundary layer interaction generates a larger region of low-momentum fluid near the suction surface in the coated cases. This additional blockage downstream of the shock results in less diffusion and higher Mach numbers in the rear of the blade passage, as illustrated by the increased size of the shaded area in which the Mach number is above 0.90.

A more quantitative view of the Mach number differences between the coated and baseline blades is provided by the streamwise Mach number distributions shown in Fig. 14, which displays the distribution of Mach number along the midpitch line, denoted by A–A. The baseline data are denoted by the * symbols, while the smooth-coated and rough-coated data are denoted by the solid and broken lines, respectively. The location and strength of both the bow shock and passage shock are nearly identical for all three cases, providing quantitative evidence that the flow field ahead of the shock and the pressure rise across the shock are not sensitive to the presence of the coatings. The baseline passage shock lies slightly downstream of that for the coated blades, which is consistent with the baseline data being acquired at a slightly higher massflow. The main difference between the three cases shown in Fig. 14 is in the levels of reacceleration and subsequent diffusion downstream of the shock. The net result is a higher Mach number at the trailing edge and a decrease in the overall diffusion between the leading edge and trailing edge. This is consistent with the reduced pressure rise observed for the coated cases.

A final comparison of the flow fields in the baseline and coated blades is provided by the blade-to-blade Mach number distributions shown for selected chordwise locations in Fig. 15. Note that although the minimum and maximum value of the ordinate scale is different for each chordwise location, the sensitivity of the ordinate scale is uniform throughout the figure (1 division = 0.1). The abscissa in each plot in Fig. 15 covers one blade pitch. The blade suction surface is on the left and the local blade section thickness is denoted by the cross-hatched region on the right. The LFA measurements are plotted at each of the 184 measurement points across the blade pitch. Regions in which there are no measurements are the result of optical blockage of the laser beam paths due to radial twist in the blade. In particular, the LFA data did not provide any information concerning separation of the suction surface boundary layer in the rear of the rotor because the LFA beams are blocked by the blade for the first 5–8 percent of pitch.

The 20 and 40 percent chord locations are upstream of the point at which the passage shock impinges on the blade suction surface. At 20 percent chord the flow near the blade surfaces shows little change in character for the coated blades relative to the baseline blade, while at 40 percent chord there is evidence of a thicker suction surface boundary layer on the coated blades. Although the shock strength (as judged by the Mach number change across the shock) is identical for all three cases, the shock is located slightly farther from the suction surface for the baseline blade than for the coated blades. As previously discussed, this is consistent with the fact that the baseline data were acquired at a slightly higher massflow than the coated blade data.

The Mach number distributions at the 65 and 90 percent chord locations provide insight into blockage changes downstream of the shock. The 65 percent chord location is just downstream of the shock impingement point on the blade suction surface. At this location the extent of the low Mach number region near the suction surface is larger for the coated cases than for the baseline case. The Mach number levels across the pitch are nearly identical, with the smooth- and rough-coated cases displaying levels just slightly above those of the baseline case. At 90 percent chord it is clear that the coated blade Mach number distributions display a significantly larger region of low Mach number fluid near the suction surface. Consistent with the increased blockage near the suction surface, the coated blade Mach number levels are higher than those of the baseline case across most of the blade pitch.

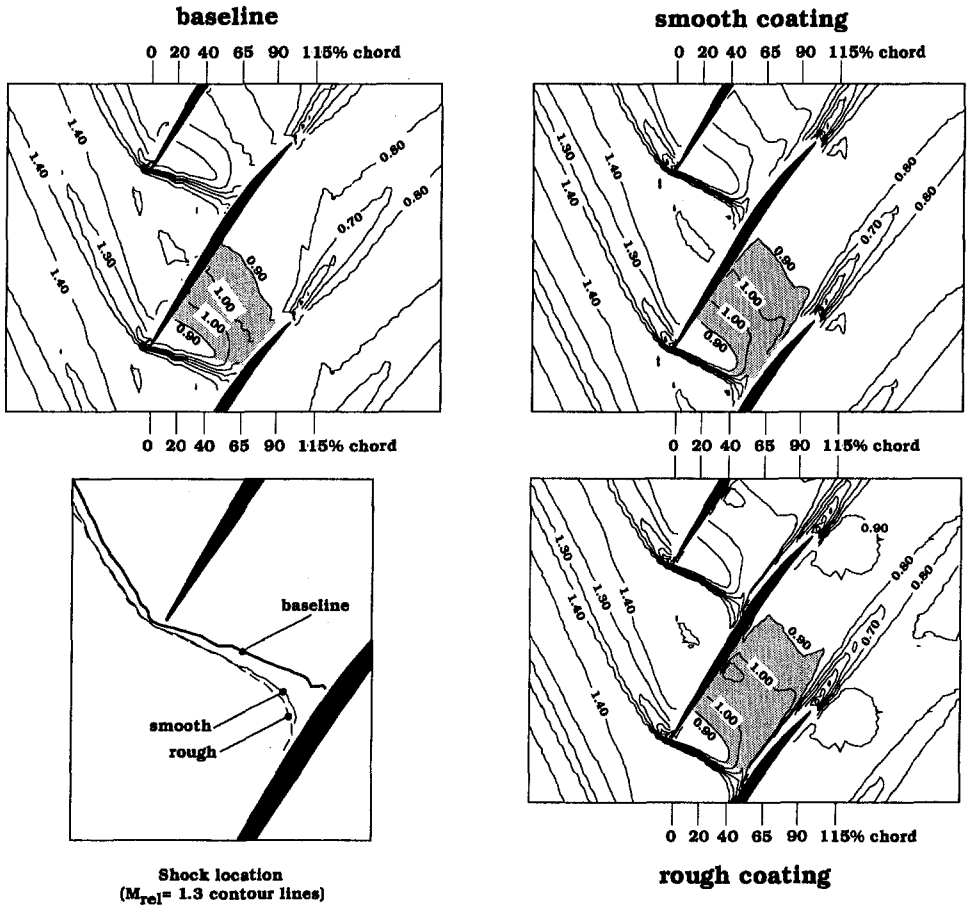

Fig. 13 Laser anemometer measurements of relative Mach number on the 70 percent span streamsurface

The final set of Mach number distributions presented in Fig. 15 was acquired at 15 percent of blade chord downstream of the trailing edge. This is the first location at which the LFA beam path is completely free from optical blockage by the blade and therefore affords us the first opportunity to obtain LFA data across the entire blade wake. The results indicate a well-behaved increase in free-stream Mach number and in wake momentum deficit (and therefore blade profile loss) as we move from the baseline case to the smooth-coated and the rough-coated cases.

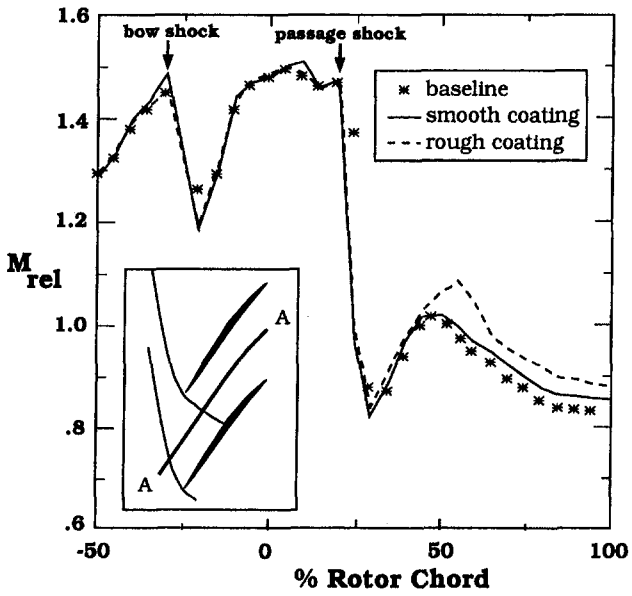

Fig. 14 Laser anemometer measurements of relative Mach number along the midpitch line, A–A, at 70 percent span

In summary, the LFA measurements indicate that the flow field upstream of the rotor passage shock and the shock itself are not altered by adding the smooth or rough coating to the blade. However, the interaction between the rotor passage shock and the suction surface boundary layer results in an increase in blockage along the suction surface downstream of the shock impingement point, which in turn results in higher Mach numbers in the rear of the blade passage.

The blockage increase is the principle flow field change that contributes to the observed performance deterioration. The pitch-averaged Mach numbers measured at 90 percent chord for the baseline and rough-coated blades are 0.840 and 0.900, respectively. The area ratio function, A/A^*, is equal to 1.024 and 1.009 for these Mach numbers. Therefore, at the relatively high exit Mach numbers that exist in Rotor 37, a blockage increase of only 1.024 − 1.009 = 0.015, or 1.5 percent, is required to account for the observed changes in Mach number in the rear of the blade passage. The shock/boundary layer interaction is a key factor in this process. This explains why the performance deterioration at part-speed conditions is much less than that at design speed, since the shock is much weaker at 80 percent speed and is not present at all at 60 percent speed.

Numerical Analysis

The purpose of the numerical analysis performed in this investigation is to complement the LFA measurements in those regions in which the measurements could not be easily acquired (near the leading edge and near the blade surface) and to provide a qualitative assessment of the flow mechanisms that cause

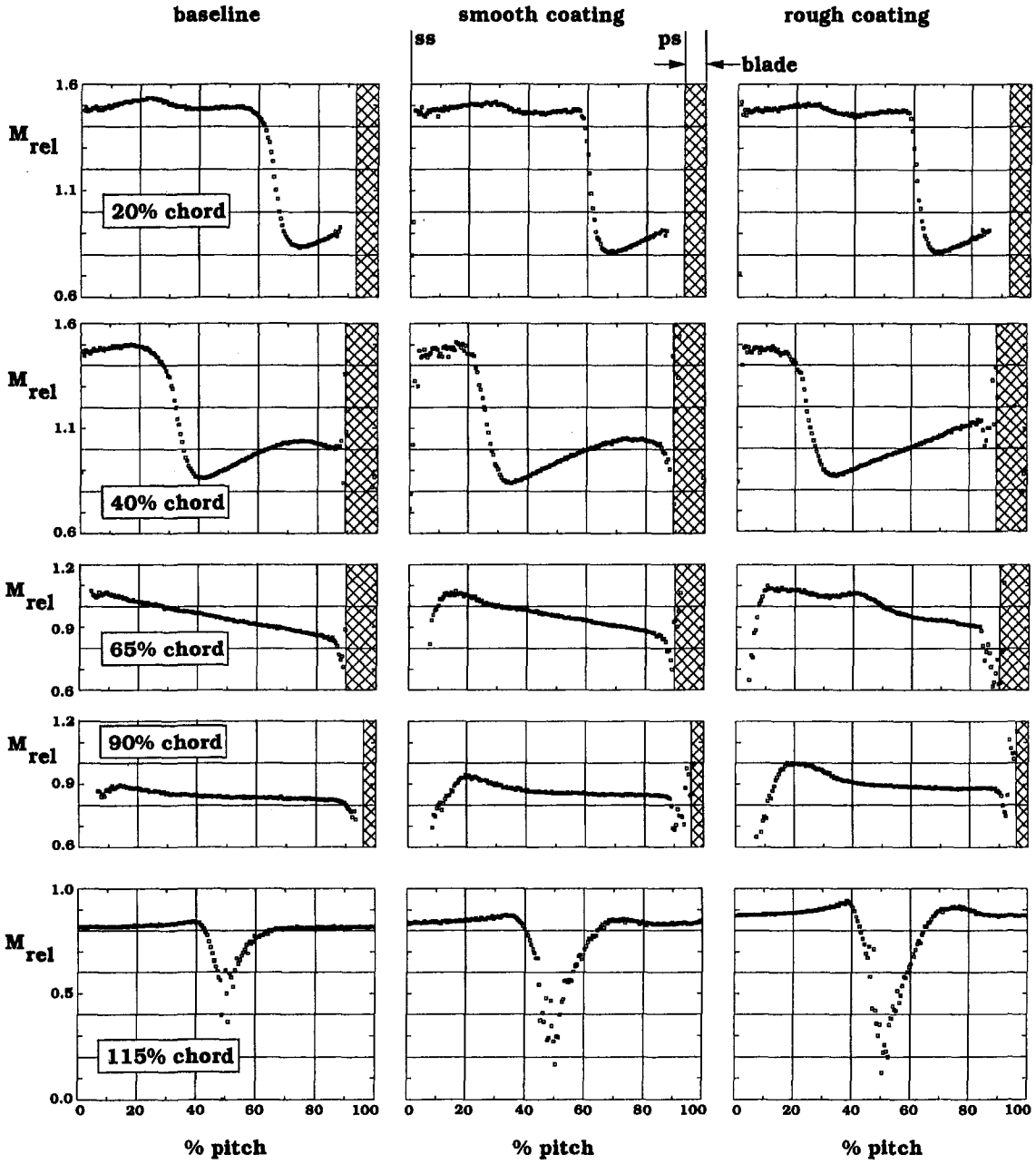

Fig. 15 Laser anemometer measurements of relative Mach number across the blade pitch on the 70 percent span streamsurface

the observed performance degradation. To meet these goals with a minimum of computational resources we chose to use a quasi-three-dimensional rather than a full-three-dimensional analysis technique. Use of a quasi-three-dimensional technique allowed us to run many different cases while varying blade thickness, grid topology, transition location, and roughness model parameters. These variations would have required an inordinate amount of computer time had they been made while using a three-dimensional analysis code. A limited number of flow field solutions were also generated using the full-three-dimensional Navier–Stokes code developed by Dawes (1988). The quasi- and full-three-dimensional solutions were compared to insure that there were no qualitative differences in the roughness/thickness effects predicted by the two approaches.

The quasi-three-dimensional results are generated using a thin-layer Navier–Stokes analysis code developed by Chima (1987). The code includes radius change and variable streamtube thickness, which were estimated from the flowpath convergence. An explicit four-stage Runge–Kutta time-marching algorithm is used with residual smoothing to improve convergence. The code employs the Baldwin–Lomax algebraic turbulence model (1978). The model is fairly accurate for attached flows, but not as good for shock-induced separation. Transition is modeled by calculating a turbulent viscosity profile along each blade-to-blade grid line, but setting the entire profile to zero if the maximum is less than a constant (usually 14) times the laminar viscosity. The model does not account for free-stream turbulence effects. The transition model was proposed in the original Baldwin–Lomax paper but it is not considered to be especially accurate. Surface roughness is modeled by increasing the turbulent mixing length using the approach of Cebeci and Chang (1978). The additional mixing length is a function of the equivalent sand grain roughness height, which is fairly small for the roughness considered here. The addition of this model to the code has been discussed in detail by Boyle and Civinskas (1991) and Boyle (1994).

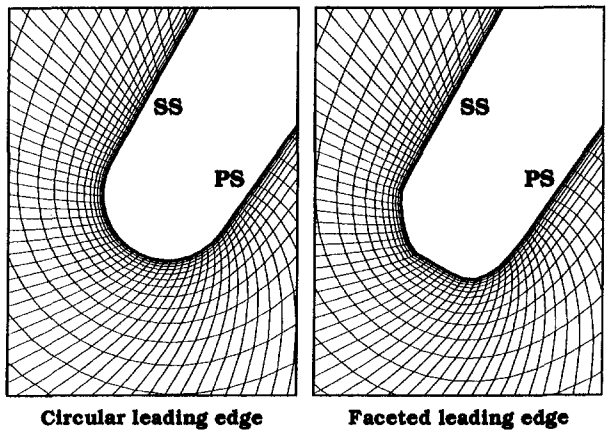

Fig. 16 CFD grid detail at the leading edge

The blade geometry at 70 percent span is used for the baseline blade profile. A C-type grid is used to provide good resolution around the blade leading edge and in the wake. The grid has 319 points around the blade with roughly 100 points on each surface and 60 points downstream. There are 45 points from the blade to midpitch, or 90 points blade-to-blade. The first grid point from the blade surface is located 0.0025 mm (0.0001 in.) from the blade surface, which corresponds to about one-tenth of the thickness of the coatings applied to the blade, or to about $y^+ = 2.5$ in turbulent wall units.

Solutions were all run for 2500 iterations, which reduced the maximum residual between four and five orders of magnitude. Solution times were about 4.5 minutes on a Cray Y-MP.

Numerical Results

Three different blade geometries were analyzed with the quasi-three-dimensional analysis code: (*i*) the baseline blade; (*ii*) the baseline blade with a constant thickness added normal to the blade surface; (*iii*) the thickened blade with a noncircular leading edge. The noncircular leading edge case was analyzed to assess the effect of leading edge manufacturing imperfections on the predicted performance. The noncircular shape used was a generic shape developed on the basis of eyelash inspections of several blades. Detailed views of the grids around the leading edges are shown in Fig. 16.

The thickness added to each blade surface was 0.025 mm (0.001 in.), which was the coating thickness measured during the experiment. The baseline and smooth-coated blade configurations were modeled by using the baseline geometry and the thickened geometry with the roughness model deactivated. The rough-coated blade was modeled by using the thickened geometry and activating the roughness model. For both the smooth and rough coatings, leading edge roughness due to particle impact damage was modeled by forcing transition at the leading edge.

The analysis code was first run assuming that the leading edge is smooth, i.e., that transition does not occur at the leading edge. For this case the analysis code predicts that transition will occur for both the baseline and thickened blades at about 36 percent chord on the suction surface, where it is probably triggered by the pressure rise through the foot of the shock which extends slightly upstream from the main shock in a classic lambda pattern. Transition is predicted at about 29 percent chord on the pressure surface. Although the transition locations predicted using the Baldwin–Lomax model are not considered to be particularly reliable, the results do indicate a sizable laminar flow region, especially on the suction surface.

The overall pressure rise characteristics predicted by the analysis for the baseline and smooth-coated blade are compared to the characteristic measured for the smooth-coated blade in Fig. 17. The purpose of Fig. 17 is to display *trends* in the predicted performance deterioration as thickness is added to the blade leading edge. The shape of the pressure rise characteristic predicted by the quasi-three-dimensional analysis will not, in general, agree with that of the actual characteristic due to limitations in the quasi-three-dimensional approach, which models three-dimensional flow effects through simple changes in radius and streamtube thickness. The measured baseline performance is therefore not presented in Fig. 17, and the measured smooth-coated performance is shown only to indicate the general *level* of the measured performance deterioration.

The three predicted characteristics shown in Fig. 17 are for the baseline blade with natural transition (*), the smooth-coated blade with natural transition (Δ), and the smooth-coated blade with transition forced at the leading edge (X). There is also a single point shown for the baseline blade with transition forced at the leading edge (flagged *). The roughness model was deactivated for all of these solutions, i.e., the blade surface was treated as being hydraulically smooth.

For a smooth leading edge the predicted performance deterioration between the baseline blade (*) and the smooth-coated blade (Δ) is far less than that observed in the experiment. On the other hand, the deterioration predicted simply by forcing either the baseline (flagged *) or the smooth-coated (X) blade boundary layer to be turbulent from the leading edge while treating the blade surface as hydraulically smooth is in closer agreement with that measured in the experiment for the smooth-coated blade. This result indicates that the performance deterioration observed for the smooth-coated blade is not due to an increase in blade thickness but rather from the boundary layer being tripped at the leading edge due to increased leading edge roughness as a result of particle impact damage. This is certainly a possibility since the smooth coating was relatively soft and therefore resulted in a smooth-coated blade that was more susceptible to damage at the leading edge than was the baseline blade.

A limited number of predictions were also generated using the full-three-dimensional Dawes code. The three-dimensional analysis was performed to investigate the impact of manufacturing tolerances on aerodynamic performance. Therefore, a thickness of 0.062 mm (0.0025 in.) was added to each surface, which represents the maximum manufacturing tolerance specified for Rotor 37 when it was fabricated. Note that this thickness was 2.5 times that added to the blade for the quasi-three-dimensional analysis. The three-dimensional analysis was performed on the baseline blade and on the thickened blade and transition was

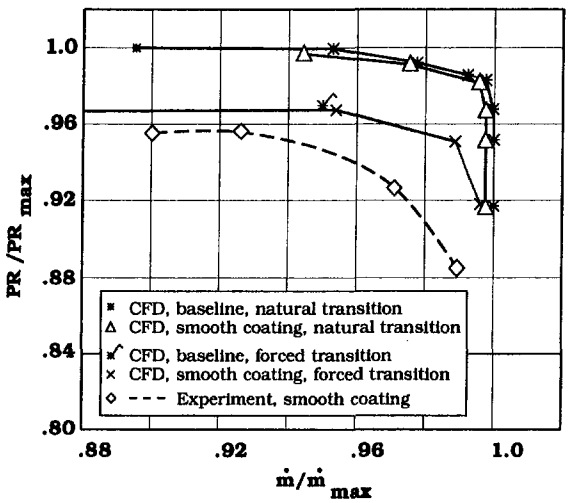

Fig. 17 Comparison between predicted and measured pressure rise versus massflow characteristics at 70 percent span for the smooth-coated blade

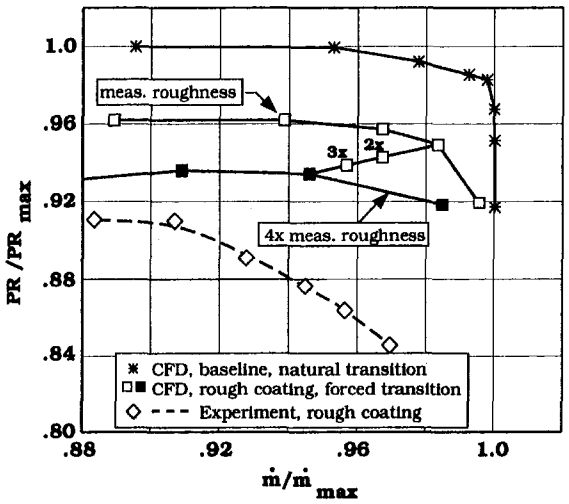

Fig. 18 Comparison between predicted and measured pressure rise versus massflow characteristics at 70 percent span for the rough-coated blade

forced at the leading edge in both cases. The results, which are not shown here, agree qualitatively with the quasi-three-dimensional results. The full-three-dimensional results indicate a stronger dependence of the choke flow rate on the addition of thickness, but this is probably due in part to the larger thickness added for the three-dimensional analysis. However, for values of $\dot{m}/\dot{m}_{\max} \leq 0.98$, the full-three-dimensional results predict only a 2 percent loss in normalized pressure ratio, which agrees with the quasi-three-dimensional predictions. Based on this exercise, we conclude that the trends in performance degradation with increased thickness predicted by the quasi-three-dimensional analysis are independent of the quasi-three-dimensional solution approach, i.e., both quasi-three-dimensional and three-dimensional analyses predict a very weak dependence between pressure rise capability and added blade thickness.

The rough-coated rotor performance was simulated by running the analysis code with the roughness model activated for equivalent surface roughness heights equal to 1, 2, 3, and 4 times that measured for the rough-coated blade in the experiment. All predictions for the rough-coated blade were generated with transition forced at the leading edge, since this procedure gave reasonable results for the smooth-coated blade case when compared to the experimental data. When the code was run in the natural transition mode with the roughness model activated, transition was still predicted to occur far from the leading edge on both the suction and pressure surface. These solutions, which are not shown here, predicted very little additional performance deterioration when compared to the smooth-coated blade solution with the boundary layer tripped at the leading edge.

The predicted results for the rough-coated and baseline blade are compared to the experimental results for the rough-coated blade in Fig. 18. As in Fig. 17, the measured performance characteristic for the rough-coated blade is included in the figure only to indicate the measured level of performance deterioration. Two different predicted characteristics are shown for the rough-coated blade. The open symbol curve represents a roughness equal to that measured in the experiment, while the solid symbol curve represents a roughness height which is four times that used in the experiment. The symbols labeled "2×" and "3×" show single points calculated for a roughness height equal to 2 and 3 times the measured roughness height. The rough-coated results shown in Fig. 18 indicate that the predicted compressor performance characteristics are sensitive to the addition of surface roughness. However, the surface roughness model significantly underpredicts the performance changes measured in the experiment.

It was quite difficult to obtain high-quality LFA measurements near the blade surface due to light reflections from the surface and optical blockage caused by blade twist. The numerical results were therefore used to provide additional insight into the flow behavior near the blade surface by using lines of constant entropy to visualize the predicted boundary layer growth. Entropy levels are highest at the blade surface and decrease to their minimum values upstream of the blade passage. The entropy levels across the shock lie between the upstream and blade surface levels. The smallest entropy level that encompasses the blades but not the shock is therefore a reasonable representation of the boundary layer edge. This entropy level is shown in Fig. 19 for the baseline, smooth-coated, and rough-coated cases. The same entropy level is used for each case. The baseline blade results are for natural transition, while the smooth and rough results are for transition forced at the leading edge. The rough-coated result is for a roughness height, which is four times that measured in the experiment. The results clearly indicate a thickening of the boundary layer near midchord, where the passage shock impinges on the blade suction surface. The trend toward increased boundary layer thickness for the coated cases agrees qualitatively with the measured trend toward higher exit Mach numbers in the coated cases. The predictions also indicate that the changes in boundary layer thickness are greater for the suction surface than for the pressure surface. This result is in qualitative agreement with the partial-coating aerodynamic performance results, which indicated less performance degradation for pressure surface roughness than for suction surface roughness.

LFA measurements did not provide information on the existence of boundary layer separation near the suction surface in the rear of the blade passage due to optical blockage of the LFA laser beams. We therefore inspected the predicted blade-to-blade Mach number distributions for the baseline and coated cases in this region to determine if the analysis code predicted boundary layer separation downstream of the shock. This exercise revealed a thin separated zone near the surface for all three cases (baseline, smooth-coated, and rough-coated) with a thickness that is relatively independent of the backpressure. The separation is limited to the first eight grid points from the surface and is therefore quite small, since the surface-normal distance

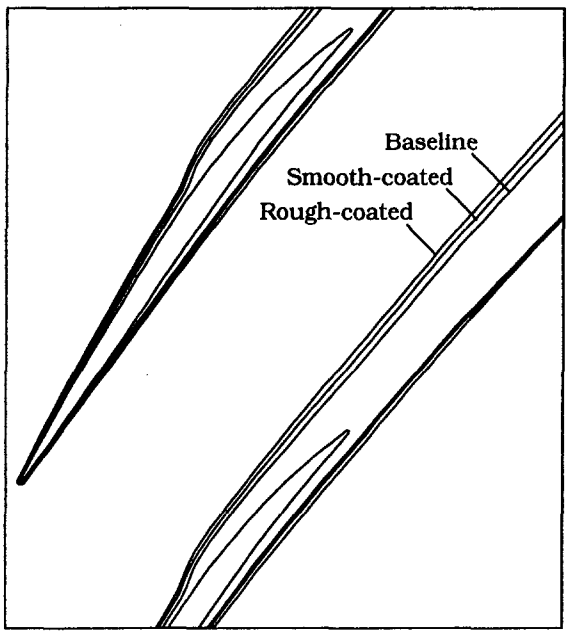

Fig. 19 Predicted boundary layer growth visualized as a locus of constant entropy

covered by these grid points corresponds to only 1 percent of the boundary layer thickness at the trailing edge.

All of the numerical results discussed above were generated using the nominal circular leading edge blade shape shown in the left half of Fig. 16. However, there are several reasons that might lead one to wonder if a circular leading edge is the proper geometry to use when trying to simulate the experimental measurements. First, the eyelash inspections of several blade leading edges showed that the leading edge is not, in general, circular (as shown in Fig. 3). Second, the coatings applied to the blade in the experimental investigation had a much lower surface hardness than the baseline metal blade, making the coated blade much more susceptible to particle impact damage at the leading edge. Finally, the smooth-coated predictions do not capture the experimental trends in performance deterioration unless transition is forced to occur at the leading edge. This raises the question: "Can a noncircular leading edge cause transition to occur earlier than it would if the leading edge were circular?"

To investigate the sensitivity of the flow field to a noncircular leading edge shape, the analysis code was run using the faceted leading edge shape shown in the right half of Fig. 16. This shape was developed on the basis of eyelash inspection of several blades. Refined grids with 449 points around the blade (about 40 points around the leading edge) were used to study leading edge effects. When run in the natural transition mode, the analysis indicates that transition still occurs on the blade surface far from the leading edge. Furthermore, the analysis indicates that the sharp corners formed by the faceted leading edge shape do not cause the formation of a separation bubble or any strong shock features. In fact the flow expands from the stagnation point all around the leading edge, and only sees a weak adverse pressure gradient when it reaches the flat part of the blade surface. Calculations were performed for operating points near choke (low incidence) and near stall (high incidence) and indicate that the noncircular leading edge shape chosen for this analysis does not have a significant impact on the predicted blade row performance at any operating condition. This issue certainly warrants further investigation using better transition models.

Conclusions

The results of this investigation indicate that adding roughness to a transonic axial-flow compressor rotor can result in a significant degradation in overall performance. The nominal coating thickness of 0.025 mm (0.001 in.) on each blade surface corresponded to an increase in leading edge thickness of 10 percent at the hub and 20 percent at the tip of the blade. The addition of a smooth coating resulted in a 4 percent loss in pressure ratio across the rotor at an operating point near design massflow. This coating did not increase roughness over the blade surface except at the leading edge, where roughness increased due to particle impact damage to the coating. The addition of a rough coating of equal thickness with a surface finish of 2.54–3.18 μm (100–125 μin.), resulted in a 9 percent loss in pressure ratio across the rotor at the same operating point. The largest degradation in pressure rise occurs over the outer half of the blade span at design speed.

When assessed at a constant pressure ratio, the adiabatic efficiency degradation at design speed is on the order of 3–6 points for the smooth coating and 6–8 points for the rough coating. Aerodynamic efficiency decreases at all speeds tested, even at fully subsonic operating conditions. At 60 percent of design speed, the effect of roughness on the blade boundary layer development is still significant, resulting in a loss in adiabatic efficiency of 1–3 points. Therefore, surface roughness should not be ignored during the manufacture or refurbishment of subsonic blading.

The conclusions of this investigation are:

1 A detailed investigation into which areas of the blade surface are most sensitive to roughness effects at design speed identified the leading edge and the front half of the suction surface as critical regions in this regard. All partially coated configurations in which the leading edge was coated suffered a significant performance degradation when compared to those for which the leading edge was uncoated. In coating the leading edge, we increased both its thickness and roughness. However, flow field predictions generated using both quasi- and full-three-dimensional Navier–Stokes codes indicate that adding thickness to the blade has little impact on performance. These facts lead to the suggestion that in the manufacture and repair of transonic axial blading, the blade leading edges should be as smooth as possible and designed to stay that way for as long as possible in service.

2 The flow field predictions generated with a quasi-three-dimensional flow solver indicate the existence of significant laminar flow regions on both the pressure and suction surface of the airfoil when the blade boundary layers are allowed to undergo natural transition. This result suggests that fan blades, which operate in a clean flow environment free of upstream blades and struts, may be more susceptible to performance deterioration due to leading edge erosion than are core compressor blades, which operate in a highly disturbed environment.

3 The simple roughness model used in the quasi-three-dimensional calculations yields the proper trends in performance deterioration but underpredicts the impact of surface roughness on performance. Reasonable agreement between flow field predictions and the experimental data for the rough-coated blade cannot be achieved by using roughness levels higher than those measured in the experiment.

4 The quasi-three-dimensional analysis of a noncircular leading edge indicates that transition at the leading edge is not triggered simply by the noncircular leading edge shape considered herein.

5 Laser anemometer measurements indicate that the sensitivity of Rotor 37 to thickness/roughness at design speed is primarily due to blockage changes in the rear of the blade passage. Coating the blade increases the suction surface boundary layer thickness upstream of the shock, which results in a significant thickening of the suction surface boundary layer downstream of the shock/boundary layer interaction. The resulting blockage reduces the overall diffusion across the blade passage, thereby reducing the pressure and temperature rise through the rotor. The rather tight throat area margin and high exit Mach numbers in Rotor 37 make it quite sensitive to small blockage changes. A rotor that features lower exit Mach numbers than Rotor 37 could therefore be expected to be less sensitive to added thickness and roughness.

Acknowledgments

The authors would like to thank the NASA Lewis Research Center for supporting the research effort reported herein, and Mr. Jerry Wood for performing the full-three-dimensional Dawes-code analysis of added thickness effects and for his helpful comments. The last author would particularly like to thank Sermatech International for their support of his participation in this research effort. Finally, the authors would like to thank Aviation Product Support Inc. for providing sample fan blades for inspection of in-service blade surface deterioration.

References

Alber, I. E., Bacon, J. W., Masson, B. S., and Collins, D. J., 1973, "An Experimental Investigation of Turbulent Transonic Viscous–Inviscid Interactions," *AIAA Journal*, Vol. 11, No. 5, pp. 620–627.

Baldwin, B. S., and Lomax, H., 1978, "Thin-Layer Approximation and Algebraic Model for Separated Turbulent Flows," AIAA Paper No. 78-257.

Boyle, R. J., and Civinskas, K. C., 1991, "Two-Dimensional Navier–Stokes Heat Transfer Analysis for Rough Turbine Blades," AIAA Paper No. 91-2129; also NASA TM 106008.

Boyle, R. J., 1994, "Prediction of Surface Roughness and Incidence Effects on Turbine Performance," ASME JOURNAL OF TURBOMACHINERY, Vol. 116, pp. 745–751.

Boynton, J. L., Tabibzadeh, R., and Hudson, S. T., 1993, "Investigation of Rotor Blade Roughness Effects on Turbine Performance," ASME JOURNAL OF TURBOMACHINERY, Vol. 115, pp. 614–620.

Cebeci, T., and Chang, K. C., 1978, "Calculation of Incompressible Rough-Wall Boundary Layer Flows," *AIAA Journal,* Vol. 16, July, pp. 730–735.

Chima, R. V., 1987, "Explicit Multigrid Algorithm for Quasi-Three-Dimensional Viscous Flows in Turbomachinery," *Journal of Propulsion and Power,* Vol. 3, No. 5, pp. 397–405.

Covey, R. R., Mascetti, G. J., and Roessler, W. U., 1978, "Examination of Commercial Aviation Operational Energy Conservation Strategies," The Aerospace Corporation, Aerospace Report No. ATR-79(7761)-1, Vol. 2.

Dawes, W. N., 1988, "Development of a 3-D Navier Stokes Solver for Application to All Types of Turbomachinery," ASME Paper No. 88-GT-70.

DOE/FAA, 1981, *Proceedings of the DOE/FAA Symposium on Commercial Aviation Energy Conservation Strategies,* Apr.

Koch, C. C., and Smith, L. H., 1976, "Loss Sources and Magnitudes in Axial-Flow Compressors," ASME *Journal of Engineering for Power,* Vol. 98, pp. 411–424.

Kramer, W. H., Paas, J. E., Smith, J. J., and Wulf, R. H., 1980, "CF6-6D Engine Short-Term Performance Deterioration," NASA CR-159830.

Liepmann, H. W., and Roshko, A., 1967, *Elements of Gasdynamics,* Wiley, New York.

Moore, R. D., and Reid, L., 1980, "Performance of a Single-Stage Axial-Flow Transonic Compressor With Rotor and Stator Aspect Ratios of 1.19 and 1.26, Respectively, and With Design Pressure Ratio of 2.05," NASA TP 1659.

Moses, J. J., and Serovy, G. K., 1951, "Effect of Blade-Surface Finish on Performance of a Single-Stage Axial-Flow Compressor," NASA RME51c09.

Nichols, C. E., Jr., 1987, "Preparation of Polystyrene Microspheres for Laser Velocimetry in Wind Tunnels," NASA TM 89163.

Reid, L., and Urasek, D. C., 1973, "Experimental Evaluation of the Effects of a Blunt Leading Edge on the Performance of a Transonic Rotor," ASME *Journal of Engineering for Power,* Vol. 95, pp. 199–204.

Reid, L., and Moore, R. D., 1978, "Design and Overall Performance of Four Highly-Loaded, High-Speed Inlet Stages for an Advanced High-Pressure-Ratio Core Compressor," NASA TP 1337.

Roelke, R. J., and Haas, J. E., 1983, "The Effect of Rotor Blade Thickness and Surface Finish on the Performance of a Small Axial Flow Turbine," ASME *Journal of Engineering for Power,* Vol. 105, pp. 377–382.

Sallee, G. P., Kruckenburg, H. D., and Toomey, E. H., 1978, "Analysis of Turbofan Engine Performance Deterioration and Proposed Follow-on Tests," NASA CR-134769.

Strazisar, A. J., Wood, J. R., Hathaway, M. D., and Suder, K. L., 1989, "Laser Anemometer Measurements in a Transonic Axial-Flow Fan Rotor," NASA TP 2879.

Suder, K. L., and Celestina, M. L., 1994, "Experimental and Computational Investigation of the Tip Clearance Flow in a Transonic Axial Compressor Rotor," ASME Paper 94-GT-365; accepted for publication in ASME JOURNAL OF TURBOMACHINERY.